AIAA-82-1094
Differences Between Actual and Predicted Pressure-Time Histories of Solid Rocket Motors

T.E. Kallmeyer and L.H. Sayer,
Thiokol/Wasatch, Brigham City, UT

AIAA/SAE/ASME
18th Joint Propulsion Conference
June 21-23, 1982/Cleveland, Ohio

DIFFERENCES BETWEEN ACTUAL AND PREDICTED PRESSURE-TIME HISTORIES OF SOLID ROCKET MOTORS

Thomas E. Kallmeyer*
Larry H. Sayer**
Thiokol Corporation/Wasatch Division
P.O. Box 524, Brigham City, Utah 84302

Abstract

The actual steady state pressure-time histories of solid rocket motors (SRMs) do not always follow the curve shape predicted by classical equations and methodology. Amplitude and time of maximum deviation from predicted pressure vary from motor to motor. Data are presented relative to this deviation for the Space Shuttle SRM which has propellant grain segments of cylindrical and star perforate configurations. Data relative to a similar condition (coning) are discussed for end burning grains.

Introduction

The solid propellant industry has for years strived to improve methods of analytically modeling the characteristics of solid rocket motors having large length-to-diameter (L/D) ratios, where the "erosive burning" caused by high gas velocities in the grain center port has been inadequately modeled a priori from either theoretical or empirical bases. Over the years, it has become increasingly evident that some motors with relatively low internal velocities, which would be expected to perform consistently with the classical equations based on uniform burning of the solid propellant grain, also exhibit differences from the predicted pressure-time trace. This deviation in pressure-time history is believed to be caused by a spatial variation in basic propellant burning rates within the cured grain, which in turn is believed to be a function of the propellant formulation and processing characteristics, the casting arrangement, and processing history. The purpose of this paper is to present data relative to the nonuniformity of ballistic properties within solid propellant grains.

Sources of Prediction Differences

The steady state pressure level of a solid rocket motor (SRM) at any point in time can be predicted by the equation

$$P = \left(\frac{C^* \rho_p \, r_{ref} \, A_b}{g \, A_t \, P_{ref}^{\,n}} \right)^{\frac{1}{1-n}}$$

Conventional methodology assumes the density (ρ_p) of the propellant to be constant throughout the grain. The characteristic velocity (C*) is a weak function of pressure and is usually input in the form,

$$C^* = C^*_{ref} \left(\frac{P}{P_{ref}} \right)^{\alpha}$$

Errors in the input values of ρ_p and C* represent a constant percentage amplitude shift in pressure level over the firing duration and do not cause a time dependent error in prediction.

The throat area (A_t) is a function of the initial throat diameter and the erosion rate ($\dot{e}$) of the throat material (or throat closure rate if, for example, a tungsten throat material is used). The throat erosion for most carbon base materials used in contemporary nozzles is almost linear with time after the first few seconds, for a given pressure level, but the erosion rate does vary with pressure in the same manner that C* varies with pressure; i.e.,

$$\dot{e} = \dot{e}_{ref} \left(\frac{P}{P_{ref}} \right)^{\beta}$$

Errors in $\dot{e}_{ref}$ or β will produce a curve shaping distortion with time, with the deviation from prediction being progressive or regressive in character.

The value of burn rate slope (n) is usually the value derived from subscale motor tests over the pressure range of interest. For most state-of-the-art hydrocarbon propellants, the burn rate-pressure relation is linear on a log-log plot; i.e.,

$$r = aP^n = r_{ref} \left(\frac{P}{P_{ref}} \right)^n$$

In cases where slope breaks occur (i.e., the slope changes abruptly at some pressure level) or the burn rate-pressure relation is curvilinear (see Fig. 1), the computational mechanics are altered, but the subscale motor derived burn rate curve shape is still assumed to apply to the full scale motor. The selection of the subscale test vehicle is dependent on prior history with the vehicle and its sensitivity to propellant changes. The scaling of burning rate from subscale to full scale motors must also include consistency in processing of propellant for testing. An example of this is shown in Fig. 2 where the burning rate of the pro-

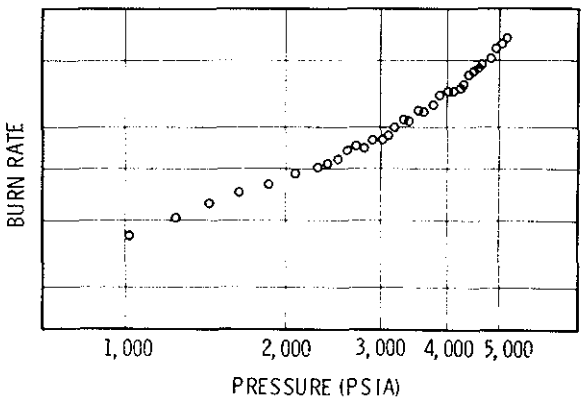

Fig. 1 Cured Strand Burn Rate Variation With Pressure

*Supervisor, Ballistics Section, Thiokol Corporation, Wasatch Division, Member AIAA
**Manager, Motor Performance Department, Thiokol Corporation, Wasatch Division

pellant, at high pressure, is shown to be a function of prebatch time. In this case, subscale motors cast at various times within the first 50 hours after prebatch, and tested at high pressure, would introduce significant scatter in burn rate scale factors.

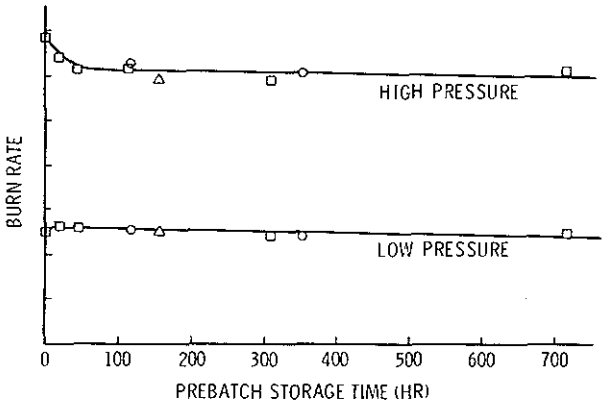

Fig. 2 Effects of Prebatch Storage Time on Subscale Motor Burn Rate

There are two basic considerations relative to reference burn rate. One is the bulk burn rate scale factor and the other is the variation of burn rate within the cured propellant grain. This spatial distribution can be caused by processing (flow conditions) and/or migration of liquid species to propellant interfaces. Burning rate unaffected by flow or migration is generally termed the bulk burning rate. Burning rates occurring at the propellant/liner interface in end burning grains are designated as edge burning rates with the ratio of edge to bulk burning rate being termed E/B.

Bulk burn rate scale factors exist between propellant samples (tested in subscale motors) obtained from subscale mixers and full scale mixers; this is often negligible but has been observed to be as great as 3 or 4%. The scale factor between subscale and full scale motors is typically within $\pm 2\%$, but has been observed to be as great as $\pm 6\%$. This scale factor uncertainty represents a potential amplitude error in the predicted pressure level, but is not time or burn distance dependent.

The burn rate variation within the cured propellant grain presents a more complex problem since it is not predictable in advance and can create a distortion in the surface area vs burn distance relationship predicted on the basis of uniform burnback. The mass generation rate, and hence the pressure time curve, will deviate from classical predictions because of both the burn rate and surface area deviations. This phenomenon has been referred to by various terms such as: Hump, BARF (Burning-rate Anomalous Rate Factor, SBRE (Surface-Burn Rate Error), and Residuals. In general, all predictability errors which are reflected in the curve shape deviations are lumped into "factors" to compensate for these deviations. This factor is the ratio of the actual to the predicted pressure, taken to the 1-n power, to relate it to an effective surface area or effective burn rate at a given time or web distance burned. This effective surface area/burn rate factor will be referred to in this paper as Hump or the Hump factor.

Ballistic Nonuniformity in End Burning Grains

As indicated earlier, spatial changes in burning rates within a propellant grain can occur due to processing or propellant ingredient migration. There are numerous techniques which can be utilized to quantify the migration effect on burning rate.

Liquid propellant species, including some commonly used plasticizers and catalysts, can move from the propellant into materials at the propellant interfaces such as insulators, inhibitors, liners, RTV coated tooling, etc. Laboratory samples can be made, aged, and then analyzed to determine mobile specie concentrations vs distance from the insulation/propellant interface. These can then be modeled to determine diffusivities. A developed model vs actual test data are shown in Fig. 3.

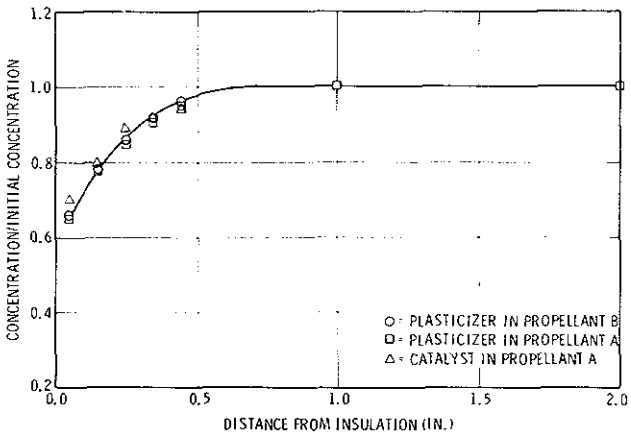

Fig. 3 Comparison of Selected Computer Model and Measured Diffusion Profiles

Migration and its impact on propellant burning rate can also be a function of the pressure at which the motor operates. This has been evident in several studies performed at Thiokol. In one study, a matrix of subscale propellant mixes was made varying the plasticizer and catalyst concentrations. Subscale motors and strands were then made and tested at two pressure levels. A linear regression of these data established the burning rate, at two different pressures, as a function of plasticizer and catalyst levels. This data evaluation indicated that at low pressure the enhancement of burning rate by the catalyst is approximately twice the depressant effect of the plasticizer. At high pressure, the depressant effect of the plasticizer is approximately five times the enhancement effect of the catalyst. This indicates that, at the lower pressure, migration of plasticizer and catalyst to the liner would leave the propellant edge with a burn rate equal to or slightly lower than the bulk burn rate. Migration of catalyst to the liner/insulation system leaves a propellant with a lower burn rate, while migration of plasticizer leaves a propellant with a high burning rate. At the high pressure, the dominant migration variable is the plasticizer which will produce an edge burning rate which is higher than the bulk burning rate.

Subscale end burning motors (5-in. diameter) were built and extinguished by rapidly depressurizing the motor while firing in an altitude cell. These subscale motors were internally stress re-

lieved as depicted in Fig. 4. These tests verified the hypothesis of chamber pressure dependent coning. A comparison of extinguished grain profiles fired at high pressure and at low pressure is presented in Fig. 5. The progression of coning in an end burning grain is depicted in Fig. 6 where identical tests have been extinguished at different times during motor operation. These high pressure extinguishment tests showed the case insulation interface burning rate to be approximately 3% higher than the bulk rate and the inhibitor interface to be approximately 6% higher than the bulk rate. Typical end burning pressure vs time traces are presented in Figs. 7 and 8, which illustrate the relative neutrality of the low pressure burning and the progressivity created by coning at the high pressure levels, respectively.

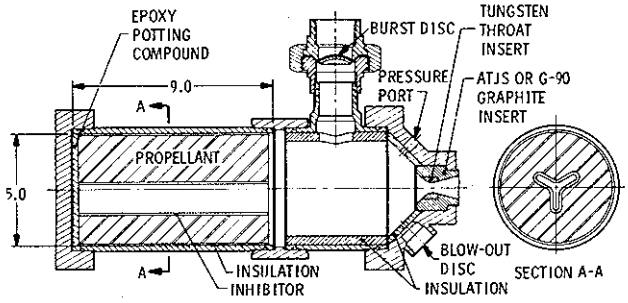

Fig. 4 Extinguishment Test Motor

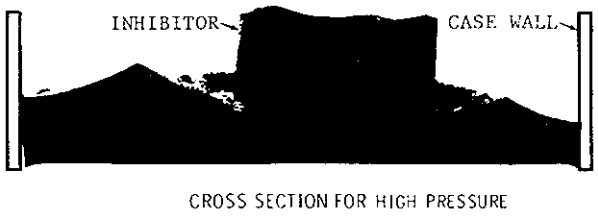

CROSS SECTION FOR HIGH PRESSURE

CROSS SECTION FOR LOW PRESSURE

Fig. 5 Comparison of Grain Burnback at Different Pressure Levels

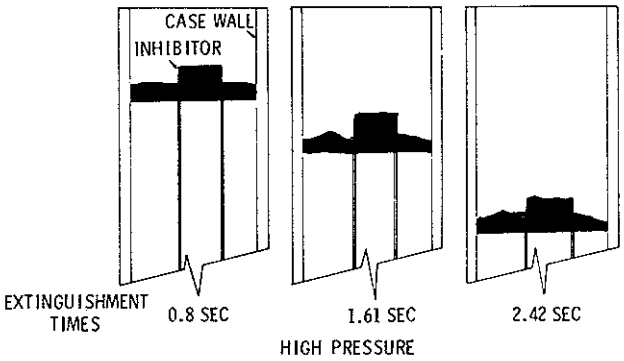

Fig. 6 Grain Surfaces of Extinguishment Motor at Various Times

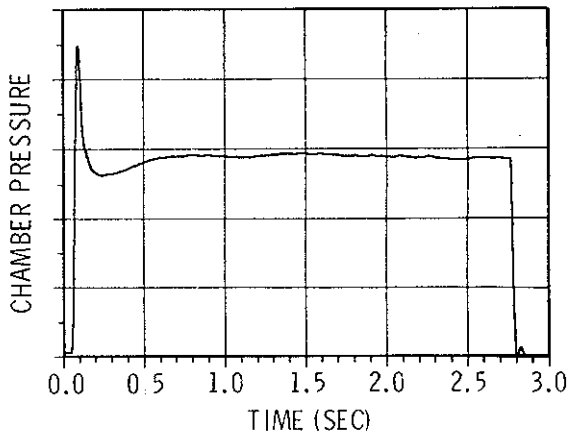

Fig. 7 Typical Low Pressure Extinguishment Pressure Trace

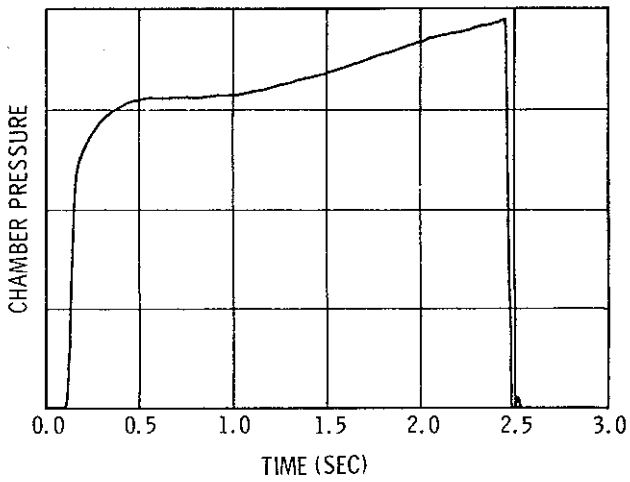

Fig. 8 Typical High Pressure Extinguishment Pressure Trace

Large Motor Experience

Thiokol's experience with the Hump characteristic has usually centered around large motors where migration cannot explain the difference between the predicted and the actual pressure trace. The Hump phenomenon is illustrated in Fig. 9. Hump is typically characterized by low (3 to 4% below predicted) initial equilibrium pressure, followed by above predicted pressure levels (typically 3 or 4%) during mid-burn, and finally lower than predicted pressure during the latter phase of burn.

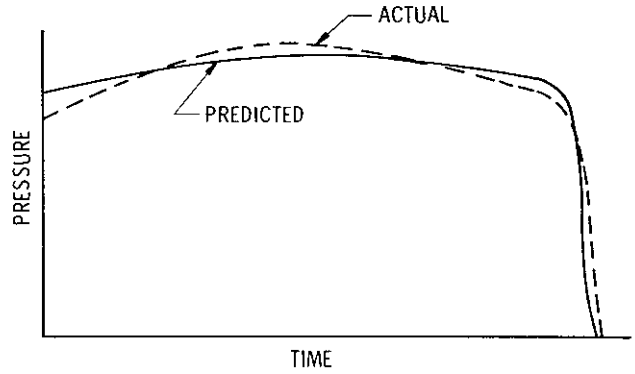

Fig. 9 Typical Hump Characteristic

The ignition transient and tailoff transient, often slower than expected, may be affected by the parameters causing Hump. The pressure-time curve shape for a given system, although not predictable in advance and different from that predicted by uniform burnback models, has proven to be reproducible once it is established. Each motor/propellant system is unique in the extent and detail in which it deviates from theoretical; i.e., each motor system has its own fingerprint or signature relative to theory.

The Hump phenomenon has usually been associated with large solid motors rather than tactical systems. One contributing reason is that tactical motors often have high length to diameter ratios (L/D), which frequently leads to high gas velocity enhancement of burning rate; i.e., erosive burning. Erosive burning does contribute to spatial nonuniformity of grain surface regression and does result in a deviation from predictions, particularly in the later phase of motor burn, if it is not accurately modeled. Generally large motors are less influenced by erosive burning, and the deviations from predicted trace shapes are believed to be more related to basic burning characteristics within the cured propellant grain. Some of the postulated contributors to Hump are listed in Table I.

TABLE I

POSTULATED CONTRIBUTORS TO HUMP

- Case/Grain Deformation at Operating Pressure
  - Distorts As-Cast Geometry
  - Strain Could Induce Burn Rate Deviation
- Propellant/Processing Characteristics
  - AP Particle Size Distribution/Orientation Between Core and Case Wall
  - Propellant Viscosity
  - Plasticizer Migration
  - Polymer Type
  - Cast/Cure Temperature Level and Uniformity
  - Cure Pressure
  - Homogeneity of Propellant
- Nozzle Throat Area History
- Unstable Combustion
- Local Gas Velocity Effects

To quantify the Hump factor after static test data have been acquired, known deviations from prefire predicted values are identified. This involves such parameters as throat erosion rate, C*, and bulk burn rate. A post-prediction is made to correct for these known and accountable deviations, and a comparison is then made between this post-prediction and the actual pressure trace. The residual pressure deviations are then most commonly translated into an effective (or pseudo-) surface area. From these pseudo-surfaces, a Hump factor can be derived in terms of A_b pseudo/A_b predicted vs percent web burned. Since burn rate and surface area are synonymous relative to their effect on pressure [$P = f(A_b \times r_b)$], this Hump factor vs percent web burned can be viewed as a surface area deviation, a burn rate deviation or a combination of the two.

Typical Hump factor vs web fraction curves are presented in Figs. 10 through 12 for a number of large solid rocket motors ranging in diameter from 37 to 260 in. Many of these motors were segmented, some had steel cases, and some had flexible cases. Most motors contained state-of-the-art hydrocarbon propellants; a few contained nitratoplasticized formulations. Virtually all of these motors exhibited some degree of Hump, but there were no identifiable parameters to correlate to the degree (amplitude) or type of Hump trace. Most of these motors were one of a kind. However, several are high production rate motors for which statistical performance variations are available. The coefficients of variation in pressure for the high production rate motors have typically been less than 2%, most of which is attributed to bulk burn rate variation, indicating that little is due to Hump factor variations.

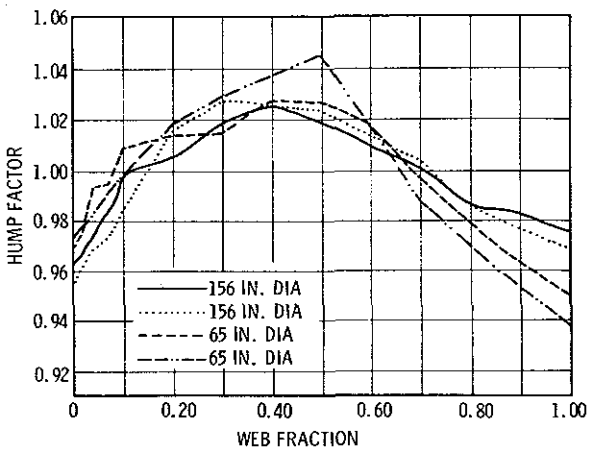

Fig. 10 Thiokol Experience With Segmented Motors

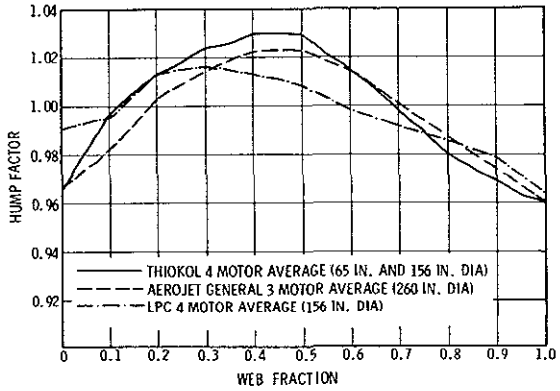

Fig. 11 Industry Experience With Large Segmented Motors

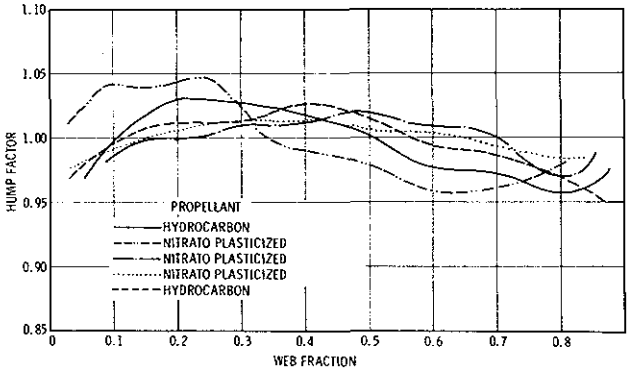

Fig. 12 Flexible Case Motors

Space Shuttle Booster Characteristics. The development of the grain configuration for the Space Shuttle Solid Rocket Motor (SRM) and the static test results of the first two development motors are discussed in Reference 1. As noted therein, the motors performed reasonably close to the predicted levels, with only a slight deviation in trace shape from that which was predicted.

The development program for the SRMs embodied the static testing of four development motors (DMs). All of these exhibited a small degree of Hump. The Hump curves generated from these four motors are shown in Fig. 13. A typical pressure-time curve is shown in Fig. 14. The general characteristics of the Hump factor and the undulations in the Hump curve are similar to those of Fig. 9.

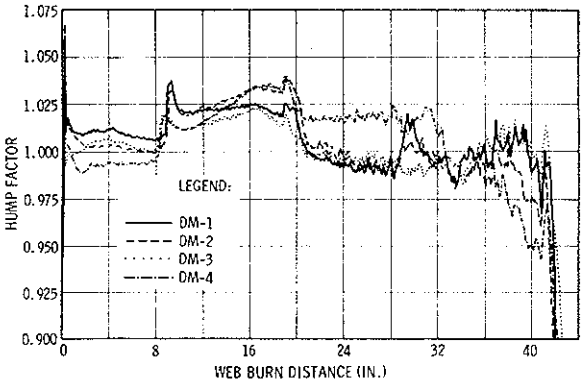

Fig. 13 Hump Curves for the Space Shuttle SRM Development Motors

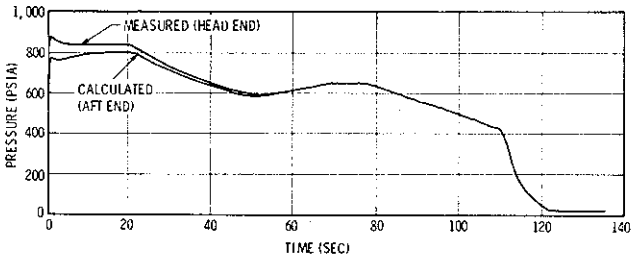

Fig. 14 Head End and Nozzle Stagnation Pressure-Time Histories

However, there are several specific differences to note. The DMs exhibit a near zero Hump factor during the first quarter of burn rather than the classical <1 factor. During the second quarter of burn, the curves reflect the typical >1 Hump factor. They then tend to shift to values at or below 1.0 during the latter half of burn. The reduction in Hump factor and the undulations in the Hump curve during tailoff are reflective of the accumulation of small inaccuracies in calculating the surface areas near web burnout.

An abrupt change in the Hump value occurs at around 20 sec (8 in. of burn), which is the time at which the forward segment star grain web burns through to the insulation and the steady state pressure level begins to decay (see Fig. 14). The time at which the pressure decay starts is later than predicted, causing the rise in the Hump curve at that time. This extended time at high pressure is interpreted to reflect a lower burn rate through the thin web of the star grain (see Fig. 15 for the SRM grain configuration). This lower burn rate near the case wall is in consonance with the generalized model of low-high-low burn rate variations with radial distance through a center perforated grain.

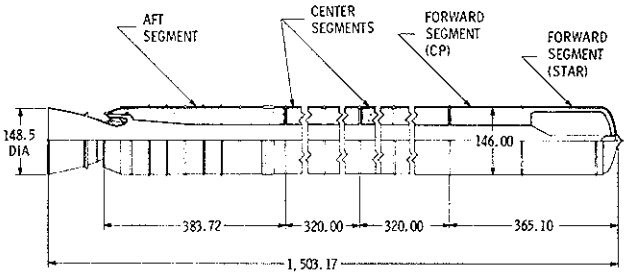

Fig. 15 Space Shuttle SRM Grain Configuration

Three qualification motors (QMs) were fabricated and static tested in the SRM program. The Hump curves for these three firings are presented in Fig. 16. The general characteristics of these curves are the same as for the DMs; however, there are some subtle differences. The average Hump curve for the first three DMs, the curve for DM-4, and the average for the three QMs are plotted on Fig. 17 as curves A, B and C, respectively. During the first 8 in. of burn, the Hump factor decreases from 1.0025 to 0.9925 to 0.985 for curves A, B, and C, respectively. Over the 9 to 18 in. burn distance, curve A is slightly progressive with an average value of about 1.025; curve C on the other hand is distinctly progressive, rising from 1.000 to about 1.028; and curve B has the progressive characteristics of curve C, but the relative amplitude of curve A. Curve A thereafter drops relatively abruptly to about 1.000 and remains about that level until near the onset of tailoff. Curve C on the other hand drops more gradually over the entire latter portion of the burn to about 0.95 at 40 in. of burn. Curve B shows characteristics of both curves A and C during this period. The general trend from development to qualification then is characterized by a reduction in the initial Hump level, a more gradual (and typical) rise to a maximum Hump factor near mid burn, and a gradual decay to values less than 1.0 by the onset of tailoff.

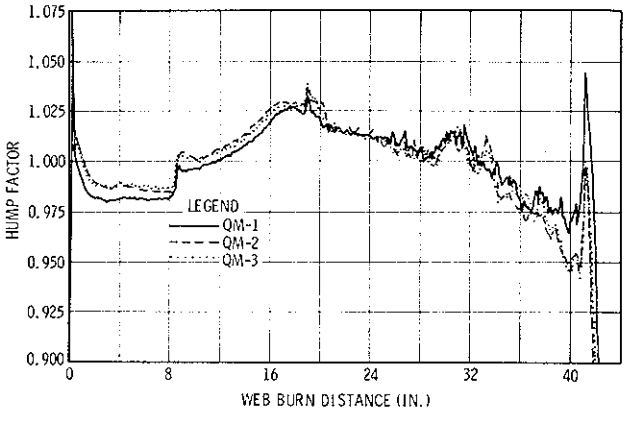

Fig. 16 Hump Curves for the Space Shuttle SRM Qualification Motors

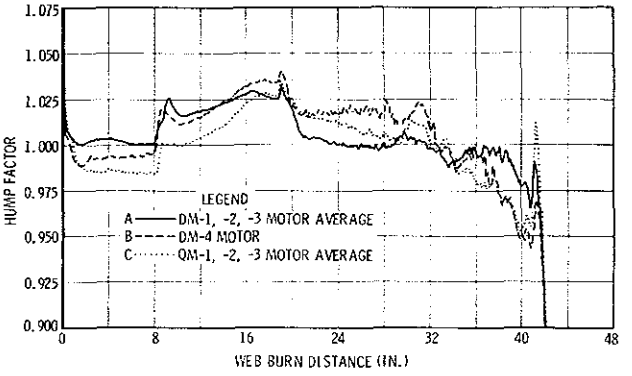

Fig. 17 Comparison of Hump Curves for Development and Qualification Motors

The observed shift is attributed to a change in motor casting tooling which was implemented between the development and qualification phases of the SRM program. The basic casting arrangement for the SRM segments is illustrated in Fig. 18. Each segment contains about forty 600 gal mixes of propellant. Each mix is made and poured sequentially into the motor at each of three circumferential locations around the segment. These three circumferential casting ports are located at a radius of 51 in., or about 50% web. The core mandrels at the casting end of the segments range from 29 to 32 in. in radius, so that the propellant falls directly into the segments and does not flow down over the core mandrels. This casting arrangement was used on the forward and two center segments of the SRMs; the aft segment differed insofar as the mandrel radius at the aft end (up during casting) is 51 in., so that the propellant first flowed onto the mandrel, which in effect functioned as a dispersion cone, and then down into the segment as a "sheet" at a radius of 51 in.

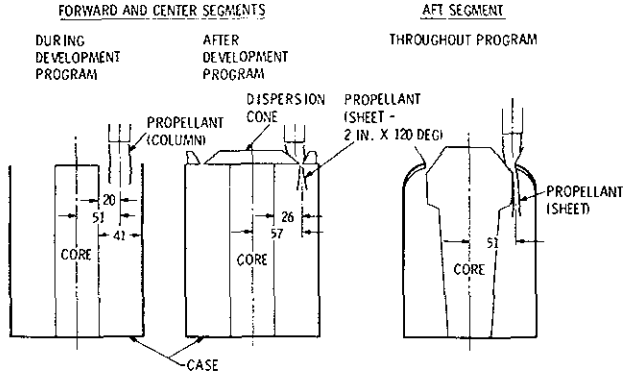

Fig. 18. SRM Segment Casting Arrangements

Prior to casting the QMs, a decision was made to add a dispersion cone to the casting tooling for the other three segments. As the tooling modifications were being implemented, one of the DM-4 center segments was cast using the modified tooling. This then gave us three motor sets having different casting configurations: the first three DMs with one segment cast with an effective dispersion cone; DM-4 having two segments cast with dispersion cones; and the QMs having all four segments cast using dispersion cones.

The Hump curves for these three motor sets were believed to reflect a change in Hump factors consistent with these processing changes. However, the changes in Hump characteristics were small and could be considered within the range of variation in Hump from motor-to-motor. With the small data base available, standard statistical tests indicated that the differences between motor sets were not sufficient to prove that the data reflect different populations. Confirmation of a shift in Hump required the acquisition of additional data.

The Hump curves from the first three sets of flight motors have now been examined to see if they substantiated the QM curve shape. Data from the six motors flown on STS-1, 2, and 3 are presented in Figs. 19 and 20. The Hump curves for the three left hand motors are plotted in Fig. 19. The right hand motor data were not plotted here since they are virtual overlays of the left hand motors until the onset of tailoff. A band representing the six flight motors, using the mean ± 3 times the standard deviation, is plotted in Fig. 20, along with the means of the first three DMs and the three QMs. These data illustrate both the excellent reproducibility of the SRMs and the consistency of the flight motors and the QMs. The Hump curves for the first three DMs fall outside this 3 sigma band, confirming the belief that the DMs and QMs are of distinct populations, and that a shift in burn characteristics occurred which is attributed to the change in casting arrangement.

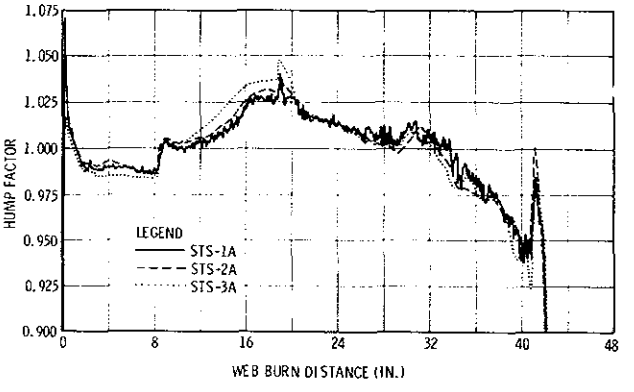

Fig. 19 Hump Characteristics for Left Hand SRMs Flown on STS-1, -2 and -3

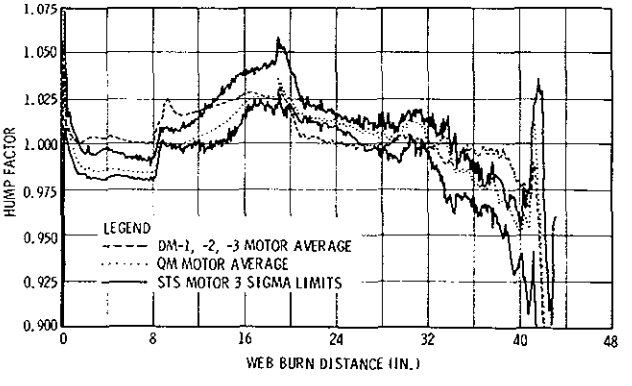

Fig. 20 Reproducibility of Flight Motors and Comparison With Static Test Motors

Conclusions

Propellant processing and ingredient migration are an inseparable part of solid rocket motor internal ballistic analysis. A spatial burning rate variation can occur in rocket motors due to the manner in which propellant is introduced at the casting location and the flow of propellant into the rocket motor case. Additionally, migration of solid propellant liquid species into inert interface materials creates a spatial propellant burn rate variation. In designing a new motor, care should be exercised in evaluating the potential for Hump. If a similar motor is not available to scale from, then tooling and ballistic performance should be designed with sufficient flexibility to accommodate some Hump effect.

Reference

1. Baker, J., "Methods Used for Space Shuttle SRB Thrust Shape Design," AIAA/SAE 14th Joint Propulsion Conference, Las Vegas, Nevada, 25-27 July 1978.